

Quantitative analysis of the electrostatic and electronic polarization energies in molecularly mixed films of organic semiconductors


Yuki Uemura,^{1,*} Syed A. Abd-Rahman,^{1,*} Susumu Yanagisawa²,³ and Hiroyuki Yoshida^{3,4,†}

¹Graduate School of Science and Engineering, Chiba University, 1-33 Yayoi-cho, Inage-ku, Chiba 263-8522, Japan

²Department of Physics and Earth Sciences, Faculty of Science, University of the Ryukyus,
1 Senbaru, Nishihara, Okinawa 903-0213, Japan

³Graduate School of Engineering, Chiba University, 1-33 Yayoi-cho, Inage-ku, Chiba 263-8522, Japan

⁴Molecular Chirality Research Center, Chiba University, 1-33 Yayoi-cho, Inage-ku, Chiba 263-8522, Japan

 (Received 9 January 2020; revised 16 July 2020; accepted 16 July 2020; published 3 September 2020)

The energy levels of organic semiconductors are primarily determined by the molecular orbital energies of constituent molecules. Recent studies have, however, shown that the energy levels can be changed by the mixing ratio of two molecules which have different permanent quadrupole moments. From the good correlation between the magnitude of the mixed film's energy shift and the constituent molecules' permanent quadrupole moment, it was noted that the molecular quadrupole plays an important role in the energy shift. In this study, ultraviolet photoelectron spectroscopy (UPS) and low-energy inverse photoemission spectroscopy (LEIPS) are applied to the mixed films of zinc phthalocyanine (ZnPc) and perfluorinated ZnPc (F₁₆ZnPc), which have permanent quadrupole moments with opposite directions. From the precisely determined ionization energies and electron affinities, we directly determine the electronic polarization energy D and electrostatic energy S as a function of mixing ratio. Furthermore, we examined the molecular orientation dependence of S and D values. D is almost independent of the mixing ratio (the difference is less than 0.2 eV over the range of mixing ratio) whereas S differs by as much as 1.6 eV. The result clearly shows that the energy levels' continuous shift by the mixing ratio originates in the electrostatic interaction, whose leading term is the charge-permanent quadrupole interaction.

DOI: [10.1103/PhysRevB.102.125302](https://doi.org/10.1103/PhysRevB.102.125302)

I. INTRODUCTION

Electronic energy levels are paramount to the performance of organic semiconductor devices such as organic light-emitting diodes (OLEDs), organic field-effect transistors, and organic solar cells (OSCs). For example, the energy level alignment at the metal and organic semiconductor interface is crucial to the charge injection and collection efficiencies at these devices' electrodes [1]. Modern OLEDs comprise multilayer structures to maximize charge injection efficiency. In OSCs, charge separation from photogenerated excitons occurs using the energy level difference at the organic/organic interface [2]. Moreover, recent studies have suggested that the trap density in organic semiconductors depends on energy levels [3].

It was believed that organic semiconductors' energy levels were determined by the molecular orbital energy of constituent molecules because the intermolecular interaction is one or two orders of magnitude smaller than that of the intramolecular interaction. Furthermore, the magnitude of intermolecular interaction only weakly depends on the materials. The dominant factors of the intermolecular interactions are electronic polarization (classical electromagnetic effect) [4] and intermolecular electronic coupling (quantum mechani-

cal effect) [5]. The magnitude of electronic polarization is 1–2 eV and is almost independent of organic materials [6]. The intermolecular electronic coupling is usually smaller than 0.1 eV and at most 0.5 eV. In fact, the energy levels of organic semiconductors are usually controlled not by the intermolecular interaction but the intramolecular interaction using the technique of organic synthesis; for example, the energy levels are lowered by halogenation of a molecule [7].

However, recent studies have shown that the energy levels of an organic semiconductor can vary as much as 1 eV depending on molecular orientation in the thin film [8–12] and the mixing ratio in blend films [13–17]. Because the magnitude of the intermolecular electronic coupling is small, the large variation of the energy levels should stem from the polarization energy.

The polarization effect is an interaction between a localized charge carrier on a single molecule and the surrounding neutral molecules and can be divided into two terms, electronic polarization (also referred to as induction or dynamic effects) and electrostatic effects [11,12,18–21]. Electronic polarization stabilizes the localized charge carrier on a molecule or an atom. The electrostatic effect, however, is the interaction between the carrier and the electrostatic potential generated by permanent charges of the surrounding molecules. When the multipole expansion is applied to the charge distribution of a nonpolar molecule, the leading term is the charge-quadrupole interaction. Whereas the electronic polarization is mostly isotropic and depends little on materials [6], the electrostatic

*These authors contributed equally to this work.

†Corresponding author: hyoshida@chiba-u.jp

effect is largely anisotropic [10], long range [11,22], and depends on a specific material. It is therefore reasonable to consider the electrostatic effect the origin of the orientation and mixing-ratio dependent energy levels. The electrostatic potential affects the charge separation mechanism in OSCs [23] and doping efficiency [24]. The open-circuit voltage can be controlled by changing the mixing ratio in the OSC donor layer [15,17].

In previous work, we have demonstrated that the magnitude of the electronic polarization and the electrostatic interaction can be experimentally evaluated from the precisely determined ionization energy, I_s , and the electron affinity, A_s . Whereas the ionization energy I_s is routinely determined using ultraviolet photoelectron spectroscopy (UPS), the precise measurement of A_s was difficult because of the lack of a suitable experimental method. Inverse photoelectron spectroscopy (IPES) is complementary to UPS and is theoretically the best method for A_s . However, the previous IPES has two serious problems of low-energy resolution and sample damage to organic material. In 2012, we developed low-energy inverse photoelectron spectroscopy (LEIPS) [25–27], which simultaneously solved these two issues by lowering the electron and photon energies and enabling measurement of the unoccupied states of the organic semiconductor with precision similar to the occupied states in UPS. From the I_s and A_s values, we determined the polarization energies for the positive and negative charges. Because the responses of electronic polarization and electrostatic energies differ depending on charge polarity [18–20], we determine the electronic polarization and electrostatic energies separately. This method has been applied to the energy levels' molecular orientation dependence [12,20]. Only the electrostatic energy depends on the molecular orientation, which implies that the orientation-dependent energy levels originate from the electrostatic effect. As the electrostatic energy can be approximated by the charge-permanent quadrupole interaction, the results can be interpreted as the molecular quadrupole moment playing a central role.

Regarding the energy shift owing to the molecular mixing, systematic studies using molecules with various permanent quadrupole moments show that the quadrupole moment plays a central role [15,17]. In this study, we will directly quantify the electrostatic energy and electronic polarization energy in the blend films using the procedure described above. For this purpose, we adopt zinc-phthalocyanine (ZnPc) and per-fluoro zinc phthalocyanine (F_{16} ZnPc). The two molecules have almost the same magnitudes of quadrupole moments with the opposite polarity (Fig. 1). The electrostatic energy generated by the molecular quadrupole moments should systematically vary as a function of the mixing ratio. Because the electrostatic energy should also depend on the molecular orientation, we also compare the blend films with edge-on and face-on orientations. The results are further interpreted using density functional theory (DFT) calculations and GW calculations [28–31].

II. EXPERIMENTAL METHODS

We purchased ZnPc and F_{16} ZnPc from Sigma-Aldrich and purified these using vacuum sublimation before use. ZnPc

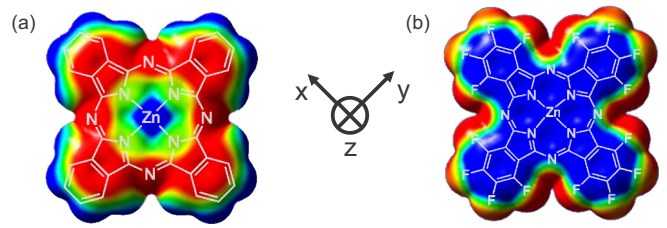


FIG. 1. Charge distribution and quadrupole tensor for (a) ZnPc and (b) F_{16} ZnPc. Surface potentials for ZnPc (top left) and for F_{16} ZnPc (top right) calculated by the DFT method of the UB3LYP/cc-PVDZ level. The blue and red are positive and negative potentials, respectively. The quadrupole tensor components for ZnPc are $Q_{xx} = Q_{yy} = 3.85 \times 10^{-39} \text{ C m}^2$, and $Q_{zz} = -7.69 \times 10^{-39} \text{ C m}^2$, while those for F_{16} ZnPc are $Q_{xx} = Q_{yy} = -4.84 \times 10^{-39} \text{ C m}^2$, and $Q_{zz} = 9.68 \times 10^{-39} \text{ C m}^2$.

and F_{16} ZnPc were coevaporated in a vacuum with 6×10^{-7} Pa pressure to prepare a blend film. The molecular orientation was controlled by the substrates. We used an indium-tin-oxide substrate (ITO)-coated glass for the edge-on orientation and a highly oriented pyrolytic graphite (HOPG) surface for the face-on orientation [9,32]. The HOPG substrates were annealed at 800 K for 10 h and cooled under the vacuum prior to use. The average film thicknesses were about 10 monolayers (MLs), that is, 10 nm for the edge-on orientation and 3 nm for the face-on orientation. The deposition rate was about 1.0 nm min^{-1} as measured by a quartz crystal microbalance. The ZnPc and F_{16} ZnPc ratio was determined by the F_{1s} and N_{1s} core level intensity ratio using x-ray photoelectron spectroscopy (XPS) with an Al $K\alpha$ excitation source (the energy $h\nu = 1486 \text{ eV}$). The uncertainty of the ratio was estimated statistically from the multiple measurements.

UPS spectra were measured with a He discharge lamp (excitation energy $h\nu = 21.22 \text{ eV}$) and a PHOIBOS-100 electron energy analyzer (SPECS). The vacuum level was determined from the cutoff energy of secondary electrons. The detailed description of the experimental setup of LEIPS is described elsewhere [33]. LEIPS spectra were measured by irradiating the sample with the electrons with energy in the range 0–4 eV and detecting photons using a bandpass filter with the center photon energy of 4.785 eV. The energy resolution was 0.43 eV as estimated by the convolution of the electron energy spread (0.33 eV) and the bandwidth of the bandpass filter (0.28 eV). The vacuum level was determined as the inflection point of the rising edge of the sample current. The sample film was not exposed to air during film preparation or measurements (*in situ* measurement). To minimize the possible effect of radiation damage, the UPS and LEIPS measurements were conducted first, followed by XPS.

The lattice constants and molecular orientations of the films were examined using grazing incidence x-ray diffraction (GIXD) at the beamline BL46XU, SPring-8. The x ray with a wavelength of 0.1 nm was incident to the sample surface at 0.12° . The reflection from the sample was detected by a two-dimensional detector (Pilatus 300 K) with an accumulation duration of 5 s. Because the diffraction from HOPG overlaps with those of ZnPc and F_{16} ZnPc, graphene on a naturally oxidized silicon wafer (purchased from Graphene Platform) was used as a substrate instead of HOPG [20]. To remove

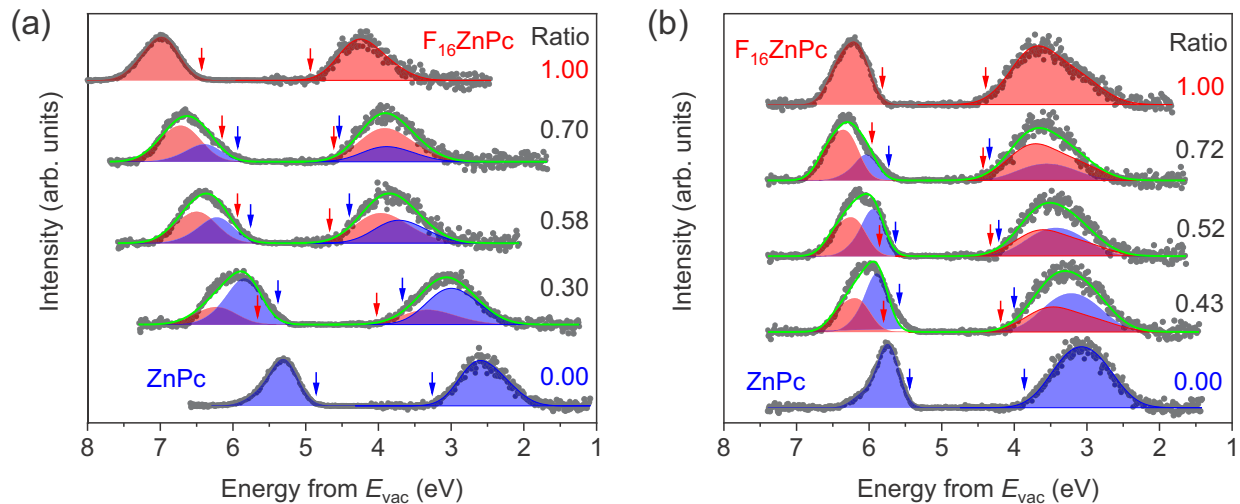


FIG. 2. UPS and LEIPS spectra of the films with (a) edge-on orientation (on ITO) and (b) face-on orientation (on HOPG). The experimental data are shown by the dots. The blue and red shaded areas are ZnPc and F_{16} ZnPc components, respectively, decomposed by Gaussian functions (see text). The sum of the fitted data in the mixed films are shown by green lines. The red (F_{16} ZnPc) and blue (ZnPc) arrows indicate the onset of HOMO and LUMO levels corresponding to I_s and A_s , respectively. The values in the panel are the molecular density ratio of F_{16} ZnPc in each film.

the contamination, the graphene film was heated at 420 K for 30 min in air, rinsed by acetone [34], and then annealed at 670 K for 4 h under vacuum.

III. RESULTS

For the prepared films, we performed XPS to determine the mixing ratio (molecular density ratio of F_{16} ZnPc in the mixed film; see Fig. S1 in the Supplemental Material [35]). The molecular orientation and lattice constants were examined using GIXD (Fig. S2) [35]. The observed diffractions could be indexed based on the reported single-crystal structures [36,37]. The crystal orientation and atomic positions confirmed that the phthalocyanine molecules stand on the ITO substrate while lying on HOPG. The lattice spacings along and normal to the substrate plane continuously change with the mixing ratio confirming the fine molecular intermixing in the mixed film (Fig. S3 and Table S1 [35]).

Figure 2 shows UPS and LEIPS spectra of the pristine and mixed films. The background signal was subtracted from the raw spectra (Fig. S4 [35]). The spectra of the low- and high-energy regions show the LEIPS and UPS spectra, respectively. The peaks observed in UPS and LEIPS were assigned to the highest occupied molecular orbital (HOMO) and lowest unoccupied molecular orbital (LUMO) -derived levels, respectively.

The peaks derived from HOMO and LUMO of the pristine ZnPc and F_{16} ZnPc films are asymmetric owing to the vibrational progression which can be well reproduced by two Gaussian functions; a Gaussian function close to the Fermi level is the dominant component while the other one far from the Fermi level is 20%–50% of the main Gaussian peak and accounts for the vibrational tail. The onset energy corresponding to I_s and A_s from both ZnPc and F_{16} ZnPc is assumed to be the energy 2σ away from the peak energy of the main Gaussian function close to the Fermi level. Note that, as

shown in Fig. 2, the determined onsets are the same as those determined by the cross point between the straight line fitted to the onset region and the baseline. I_s of pristine ZnPc on ITO and HOPG and F_{16} ZnPc on ITO and HOPG agree with previously reported UPS data [17].

We then fitted the peaks of the HOMO and LUMO of the mixed film with the reproduced peaks from both components, ZnPc and F_{16} ZnPc. In the procedure, the area ratio between the reproduced peak of ZnPc and F_{16} ZnPc was fixed to match the ratio obtained from the XPS results. I_s of the component of ZnPc with the edge-on orientation shifted continuously from 4.85 to 5.93 eV as the mixing ratio changed from 0 to 0.70. Similarly, I_s of the F_{16} ZnPc component shifted continuously from 5.64 to 6.43 eV as the mixing ratio changed from 0.30 to 1.00. The results agree with the previously reported UPS data [15]. A_s of ZnPc shifted continuously from 3.26 to 4.56 eV and A_s of F_{16} ZnPc shifted continuously from 4.02 to 4.94 eV. Regarding the face-on orientation on HOPG, I_s of the ZnPc component shifted continuously from 5.44 to 5.73 eV and A_s from 3.86 to 4.34 eV when the mixing ratio changes from 0 to 0.72. Similarly, I_s of the F_{16} ZnPc component shifts continuously from 5.80 to 5.82 eV and A_s from 4.19 to 4.39 eV when the mixing ratio changes from 0.43 to 1.00. In both orientations, the band gaps are little affected by the mixing. This finding suggests that the electrostatic energy predominantly affects the energy shift [20].

IV. DISCUSSION

We evaluate electronic polarization energy D and electrostatic energy S from the determined I_s and A_s according to the energy relation schematically shown in Fig. 3 [20]. The polarization energies for holes P_+ and for electrons P_- are obtained as the difference between ionization energy in the gas phase I_g (electron affinity in the gas phase A_g) and ionization energy in the solid phase I_s

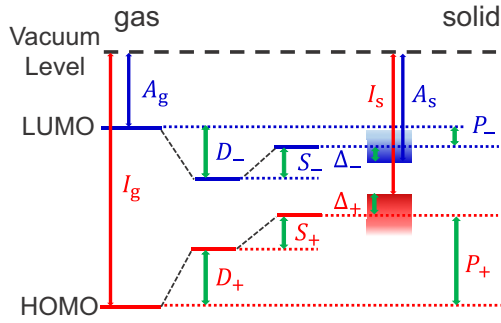


FIG. 3. Energy level diagram showing the relationship between ionization energy and electron affinity in the gas and solid phases.

(electron affinity in the solid phase A_s) with correction for the intermolecular electronic coupling Δ_{\pm} (the plus and minus signs correspond to HOMO and LUMO derived bands, respectively) [27],

$$P_+ = I_g - I_s - \Delta_+, \quad P_- = A_s - A_g - \Delta_-. \quad (1)$$

The polarization energies P_{\pm} can be divided into the electronic polarization energy D_{\pm} and electrostatic energy S_{\pm} (the plus and minus signs correspond to the hole and electron, respectively). As the electronic polarization always works to stabilize the system whichever the polarity is, we assume $D_+ = D_- \equiv D$. On the other hand, the electrostatic energies

are the Coulomb interaction energies. Since the sign of these energies alternates depending on the polarity of the charge, we can assume $S_+ = -S_- \equiv S$. Thus, the absolute values of D and S can be determined from obtained I_s , I_g , A_s , and A_g according to Eq. (1),

$$D = (P_+ + P_-)/2, \quad S = (P_+ - P_-)/2. \quad (2)$$

To calculate D and S , the values of I_g , A_g , and Δ_{\pm} are required. The experimental values are only available for I_g (6.39 eV) of ZnPc [38] and Δ_{\pm} (about half of the bandwidth, 48 meV for ZnPc and 60 meV of F_{16} ZnPc) [39]. As demonstrated previously, the calculated values agree with the experimental values [38]. Thus, we use the values calculated using DFT with the HSE06/spaug-cc-PVTZ level on the GAUSSIAN 16 program [40]. We obtained $I_g = 6.29$ eV and $A_g = 2.00$ eV for ZnPc and $I_g = 7.06$ eV and $A_g = 2.86$ eV for F_{16} ZnPc. The corrections by the intermolecular electronic coupling were assumed to be half of the bandwidth, $\Delta_+ = 120$ meV, $\Delta_- = 125$ meV for ZnPc and $\Delta_+ = 310$ meV, $\Delta_- = 170$ meV for F_{16} ZnPc. The calculated values of I_g [38] for ZnPc agreed with the experimental data.

The obtained electronic polarization energy D and electrostatic energy S for ZnPc and F_{16} ZnPc are shown in Fig. 4 as a function of the mixing ratio. The variation of D for both ZnPc and F_{16} ZnPc is less than 0.2 eV in the mixed films with edge-on orientation and 0.1 eV with face-on orientation. This result is comprehensible as the electronic polarization energy of

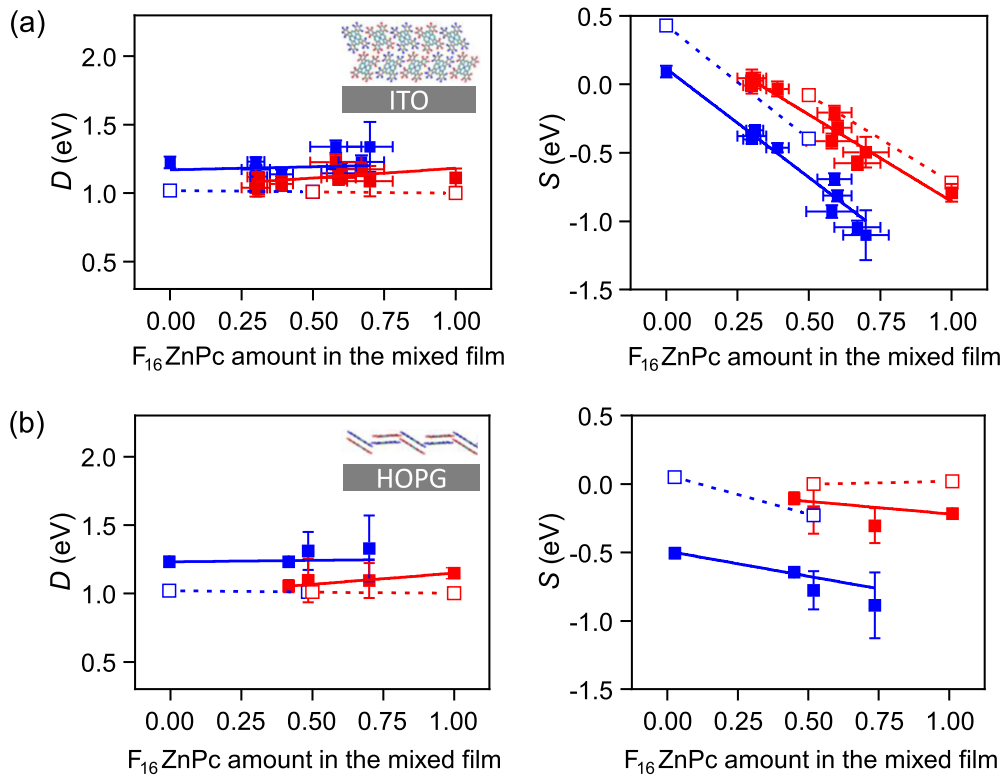


FIG. 4. Electronic polarization energy (left panel) and electrostatic energy (right panel) of the mixed films with (a) edge-on and (b) face-on orientation as a function of the molecular density ratio of F_{16} ZnPc in the mixed film. The circles show experimental data. The open squares show calculated data. The solid and dashed lines are the best-fit results to the experimental and calculated data, respectively. The uncertainties are the fitting errors in the decomposition by the Gaussian functions (see Fig. 2). The insets in the left panels are the images of standing and lying orientation of the 50% blend (see Fig. S6 in the Supplemental Material [35] for details).

organic solids is almost constant regardless of the molecules [6]. The electronic polarization energy is also almost independent of the molecular orientation. For ZnPc, the magnitude of D is 1.19 ± 0.01 eV with edge-on orientation and 1.24 ± 0.02 eV with face-on orientation. For F_{16} ZnPc the electronic polarization energy is slightly lower, 1.12 ± 0.01 eV with edge-on orientation and 1.11 ± 0.03 eV with face-on orientation. This is understood from the smaller relative permittivity of the fluorine-substituted compound than of the nonsubstituted compound [41].

Conversely, from the linear fit we calculated that S changes by 1.11 ± 0.09 eV for ZnPc between 0 and 0.70 of the mixing ratio and 0.89 ± 0.10 eV for F_{16} ZnPc between 0.30 and 1.00 of the mixing ratio in the mixed films with edge-on orientation [Fig. 4(a)]. Similarly, with face-on orientation [Fig. 4(b)], S changes by 0.26 ± 0.05 eV for ZnPc between 0 and 0.72 in the mixing ratio and 0.10 ± 0.05 eV for F_{16} ZnPc between 0.43 and 1.00 in the mixing ratio. As ZnPc and F_{16} ZnPc are nonpolar molecules, the leading term of the electrostatic energy is the charge-permanent quadrupole interaction when the multipole expansion is applied. In fact, the calculated charge distributions and quadrupole tensors are opposite between ZnPc and F_{16} ZnPc (Fig. 1). The present result is consistent with the previous argument that the interaction with the surrounding quadrupole field changed and continuous energy level shifts were observed by changing the ratio of the two molecules. The electrostatic interaction is strongly anisotropic and leads to a large difference in the magnitude of S depending on the molecular orientation. In the pristine ZnPc film, the electrostatic energy S is 0.09 ± 0.04 eV with edge-on orientation and -0.50 ± 0.04 eV with face-on orientation. In F_{16} ZnPc, the electrostatic interaction is -0.79 ± 0.07 eV with edge-on orientation and -0.22 ± 0.03 eV with face-on orientation. The observed mixing ratio dependence is large in the edge-on orientation. This can be understood from the large charge-quadrupole interaction along the molecular stacking direction.

In previous work, we demonstrated that the electrostatic energy S is calculated by the DFT method while the electronic polarization energy D can be calculated as the GW correction [20,28–31]. We apply the same calculation to 1–3 ML of the pristine and mixed (ratio of 1:1) films of ZnPc and F_{16} ZnPc. The 1–3-ML slabs were generated based on the single-crystal structures (Figs. S5 and S6 in the Supplemental Material [35]). For the mixed films, we tried the single-crystal structures of both ZnPc and F_{16} ZnPc by replacing adjacent molecules with F_{16} ZnPc or ZnPc molecules. Figure S7 [35] shows the electrostatic energies as a function of thickness of the molecular layer in the slab.

The electronic polarization energy D was calculated for the pristine bulk and $D_+ = D_-$ is assumed. The D of the mixed film was estimated as an average of those of the pristine films. The magnitude of D for both molecular orientations is around 1 eV, which is in excellent agreement with the experimental values. This implies that the electronic polarization is well described by the GW approximation. This essentially features quasiparticle or charged excitation in solids, that is, a complex of an injected charge (hole or electron) and surrounding polarization clouds [42]. The calculated D of the pristine films are similar to those of the 6,13-pentacenequinone crystals

obtained at the same level of theory [20], which agrees with previous observations [6]. The calculation predicts smaller difference between ZnPc and F_{16} ZnPc compared with the experimental tendency. This might be because of other interactions that are ignored during the calculation for mixed films.

Regarding the electrostatic energy S , the magnitude of the calculated electrostatic energies for the hole S_+ and the electron S_- are different by less than only 0.1 eV (Fig. S7 [35]). The calculated result assures our assumption $S_+ = -S_- = S$ used in the derivation of Eq. (2). Because the calculated S_+/S_- depends on the orbital energies [20], the slight difference may come from the different nature of the HOMO- and LUMO-derived bands, such as the different spatial distribution and the nodal structure of the orbitals. The results in Fig. S7 [35] show little thickness dependence, which suggests that the electrostatic interaction is mostly within the two-dimensional single layer and the interlayer interaction is small or canceled out. As reported previously, the charge-quadrupole interaction along the molecular stacking direction dominates in phthalocyanines whereas the interlayer interaction is compensated in the lying orientation when the lateral dimension exceeds 100 nm [17]. The present calculation is consistent with the report. On close inspection, the mixed film with the face-on orientation calculated in the F_{16} ZnPc lattice shows a slight anomaly at 1 ML. In this structure, the two molecules in the unit cell take different tilting angles, which affects the electrostatic energy because of the direction of the quadrupole moment.

The electronic polarization of the HOMO- and the LUMO-derived bands requires further attention. Given that the slightly different S_+ and S_- may come from the different natures of the HOMO- and LUMO-derived bands, D_+ and D_- may also differ ($D_+ = D_-$ was assumed in this study). The electronic polarization is typically the electrostatic interaction stabilizing a molecular ion in a molecular array, which depends on change in the charge density around the molecular ion site [11] and should therefore depend on the nature of the orbitals therein. To describe D_+ and D_- separately at the GW level of theory, it is necessary to explicitly treat the slab of the thin film. That should be left for future work, with further technical requirements such as truncation of the artificial long-ranged screened Coulomb interaction between the neighboring unit cells along the surface normal [43].

Figure 4 compares the experimental and calculated energies. As we found little thickness dependence in the calculation, we show the calculated values for 3 ML (the experimental results are for about 10 ML). As for the structure of the mixed film, the F_{16} ZnPc lattice is shown because no discernible difference was found in the 3-ML slabs. The experimental tendencies are reproduced excellently by the calculation, which indicates that the methods used in the analysis of the experimental data and calculation are sufficiently high to evaluate the electrostatic energies that depend on both the mixing ratio and the molecular orientation. The systematic S difference of 0.2–0.5 eV between the experimental and calculated results may be caused by the effect of the substrate or the imperfection of the crystalline structure in the experiments. The limited accuracy of the calculation for I_g and A_g also affects this because a very large basis set is necessary for quantitative accuracy.

To further examine the effect of the film thickness on D and S , we performed UPS and LEIPS measurements for a mixed monolayer film of copper phthalocyanine (CuPc) and perfluoro CuPc (F_{16} CuPc) with the standing orientation [35]. The films were prepared on a naturally oxidized silicon wafer (SiO_2). The mixing ratio and the molecular orientation were confirmed by XPS and GIXD, respectively. From UPS and LEIPS measurements (Fig. S10 [35]), we evaluated D and S as shown in Fig. S11 [35]. The results are quantitatively similar to those of 10 ML of mixed films of ZnPc and F_{16} ZnPc. The electronic polarization energies D are almost independent of the mixing ratio while the electrostatic energy S changes 1.52 ± 0.20 eV for CuPc and 1.28 ± 0.05 eV for F_{16} CuPc with mixing ratio from 0.00 to 1.00. The variation in S is a little larger in CuPc/ F_{16} CuPc than in ZnPc/ F_{16} ZnPc (1.21 ± 0.09 eV for ZnPc and $1.34 \pm .05$ eV for F_{16} ZnPc from mixing ratio 0.00 to 1.00). This finding is consistent with the larger quadrupole moment of CuPc ($Q_{xx} = 4.16 \times 10^{-39}$ C m², $Q_{yy} = 4.16 \times 10^{-39}$ C m², $Q_{zz} = -8.32 \times 10^{-39}$ C m²) compared with that of ZnPc ($Q_{xx} = 3.85 \times 10^{-39}$ C m², $Q_{yy} = 3.85 \times 10^{-39}$ C m², $Q_{zz} = -7.69 \times 10^{-39}$ C m²) calculated by the UB3LYP/cc-PVDZ level.

V. CONCLUSION

We examined both the ionization energy I_s and electron affinity A_s in multilayer films with different ZnPc and F_{16} ZnPc mixing ratios. We also controlled molecular orientations using ITO and HOPG substrates. We observed a continuous shift of both HOMO and LUMO peaks while the band gaps do not change significantly with the ZnPc and F_{16} ZnPc mixing ratio. Using the method reported previously [20], the electronic polarization energy D and electrostatic energy S are determined. The electronic polarization energy D was about 1 eV which is almost independent of the mixing ratio or molecular orientation with the variation less than 0.2 eV. Conversely,

the electrostatic energy S shows larger dependence on the mixing ratio; S varies by 1.59 ± 0.13 eV for ZnPc and 1.27 ± 0.14 eV for F_{16} ZnPc with the edge-on orientation while it varies by 0.36 ± 0.07 eV for ZnPc and 0.18 ± 0.08 eV for F_{16} ZnPc with the face-on orientation over the mixing ratio between 0 and 1. As D is approximated by the energy of charge-quadrupole moment interaction, the present results provide evidence that the continuous shift of energy levels by the mixing ratio is indeed caused by the molecular permanent quadrupole. In addition, we demonstrated these interaction energies can be quantified experimentally using a combination of UPS and LEIPS.

ACKNOWLEDGMENTS

The authors thank Dr. Kyohei Nakano and Dr. Keisuke Tajima at RIKEN for kindly measuring XPS during the difficult time due to the COVID-19 pandemic. Professor Itaru Osaka at Hiroshima University and Dr. Tomoyuki Koganezawa at Japan Synchrotron Radiation Research Institute (JASRI) are acknowledged for GIXD measurement. The authors would like to thank Yoshitada Morikawa and Ikutaro Hamada of Osaka University for providing us with the pseudopotentials used in the DFT and the GW calculations. GIXD experiments were performed at the BL46XU of SPring-8 with the approval of the JASRI (Proposal No. 2017B1831). This research was supported by JSPS KAKENHI Grants No. 26288007, No. 26105011, and No. 16KK0115 and by the “Joint Usage/Research Center for Interdisciplinary Large-Scale Information Infrastructures” and “High Performance Computing Infrastructure” in Japan (Project ID No. jh190062-NAH). The first-principles calculations were conducted at the Supercomputer Center, the Institute for Solid State Physics, The University of Tokyo and the Cyberscience Center, Tohoku University.

-
- [1] H. Ishii, K. Sugiyama, E. Ito, and K. Seki, Energy level alignment and interfacial electronic structures at organic/metal and organic/organic interfaces, *Adv. Mater.* **11**, 605 (1999).
 - [2] C. J. Brabec, N. S. Sariciftci, and J. C. Hummelen, Plastic solar cells, *Adv. Funct. Mater.* **11**, 15 (2001).
 - [3] N. B. Kotadiya, A. Mondal, P. W. M. Blom, D. Andrienko, and G. J. A. H. Wetzelaer, A window to trap-free charge transport in organic semiconducting thin films, *Nat. Mater.* **18**, 1182 (2019).
 - [4] L. Lyons and F. Gutmann, *Organic Semiconductors* (John Wiley and Sons, New York, 1967).
 - [5] N. Ueno and S. Kera, Electron spectroscopy of functional organic thin films: Deep insights into valence electronic structure in relation to charge transport property, *Prog. Surf. Sci.* **83**, 490 (2008).
 - [6] N. Sato, K. Seki, and H. Inokuchi, Polarization energies of organic solids determined by ultraviolet photoelectron spectroscopy, *J. Chem. Soc., Faraday Trans. 2* **77**, 1621 (1981).
 - [7] M. L. Tang and Z. Bao, Halogenated materials as organic semiconductors, *Chem. Mater.* **23**, 446 (2011).
 - [8] S. Duhm, G. Heimel, I. Salzmann, H. Glowatzki, R. L. Johnson, A. Vollmer, J. P. Rabe, and N. Koch, Orientation-dependent ionization energies and interface dipoles in ordered molecular assemblies, *Nat. Mater.* **7**, 326 (2008).
 - [9] W. Chen, H. Huang, S. Chen, Y. L. Huang, X. Y. Gao, and A. T. S. Wee, Molecular orientation-dependent ionization potential of organic thin films, *Chem. Mater.* **20**, 7017 (2008).
 - [10] G. Heimel, I. Salzmann, S. Duhm, and N. Koch, Design of organic semiconductors from molecular electrostatics, *Chem. Mater.* **23**, 359 (2011).
 - [11] B. J. Topham and Z. G. Soos, Ionization in organic thin films: Electrostatic potential, electronic polarization, and dopants in pentacene films, *Phys. Rev. B* **84**, 165405 (2011).
 - [12] H. Yoshida, K. Yamada, J. Tsutsumi, and N. Sato, Complete description of ionization energy and electron affinity in organic solids: Determining contributions from electronic polarization, energy band dispersion, and molecular orientation, *Phys. Rev. B* **92**, 075145 (2015).
 - [13] I. Salzmann, S. Duhm, G. Heimel, M. Oehzelt, R. Kniprath, R. L. Johnson, J. P. Rabe, and N. Koch, Tuning the ionization energy of organic semiconductor films: The role of intramolecular polar bonds, *J. Am. Chem. Soc.* **130**, 12870 (2008).

- [14] M. L. Tietze, W. Tress, S. Pfützner, C. Schünemann, L. Burtone, M. Riede, K. Leo, K. Vandewal, S. Olthof, P. Schulz, and A. Kahn, Correlation of open-circuit voltage and energy levels in zinc-phthalocyanine: C60 bulk heterojunction solar cells with varied mixing ratio, *Phys. Rev. B* **88**, 085119 (2013).
- [15] M. Schwarze, W. Tress, B. Beyer, F. Gao, R. Scholz, C. Poelking, K. Ortstein, A. A. Günther, D. Kasemann, D. Andrienko, and K. Leo, Band structure engineering in organic semiconductors, *Science* **352**, 1446 (2016).
- [16] N. Ueno, Tuning organic band structures with Coulomb interactions, *Science* **352**, 1395 (2016).
- [17] M. Schwarze, K. S. Schellhammer, K. Ortstein, J. Benduhn, C. Gaul, A. Hinderhofer, L. Perdígón Toro, R. Scholz, J. Kublitski, S. Roland, M. Lau, C. Poelking, D. Andrienko, G. Cuniberti, F. Schreiber, D. Neher, K. Vandewal, F. Ortmann, and K. Leo, Impact of molecular quadrupole moments on the energy levels at organic heterojunctions, *Nat. Commun.* **10**, 2466 (2019).
- [18] N. Sato, H. Inokuchi, and E. A. Silinsh, Reevaluation of electronic polarization energies in organic molecular crystals, *Chem. Phys.* **115**, 269 (1987).
- [19] P. J. Bounds and R. W. Munn, Polarization energy of a localized charge in a molecular crystal. II. Charge-quadrupole energy, *Chem. Phys.* **59**, 41 (1981).
- [20] K. Yamada, S. Yanagisawa, T. Koganezawa, K. Mase, N. Sato, and H. Yoshida, Impact of the molecular quadrupole moment on ionization energy and electron affinity of organic thin films: Experimental determination of electrostatic potential and electronic polarization energies, *Phys. Rev. B* **97**, 245206 (2018).
- [21] S. M. Ryno, C. Risko, and J.-L. Brédas, Impact of molecular orientation and packing density on electronic polarization in the bulk and at surfaces of organic semiconductors, *ACS Appl. Mater. Interfaces* **8**, 14053 (2016).
- [22] C. Poelking, M. Tietze, C. Elschner, S. Olthof, D. Hertel, B. Baumeier, F. Würthner, K. Meerholz, K. Leo, and D. Andrienko, Impact of mesoscale order on open-circuit voltage in organic solar cells, *Nat. Mater.* **14**, 434 (2015).
- [23] C. Poelking and D. Andrienko, Design rules for organic donor-acceptor heterojunctions: Pathway for charge splitting and detrapping, *J. Am. Chem. Soc.* **137**, 6320 (2015).
- [24] R. Warren, A. Privitera, P. Kaienburg, A. E. Lauritzen, O. Thimm, J. Nelson, and M. K. Riede, Controlling energy levels and Fermi level en route to fully tailored energetics in organic semiconductors, *Nat. Commun.* **10**, 5538 (2019).
- [25] H. Yoshida, Near-ultraviolet inverse photoemission spectroscopy using ultra-low energy electrons, *Chem. Phys. Lett.* **539–540**, 180 (2012).
- [26] H. Yoshida, Measuring the electron affinity of organic solids: An indispensable new tool for organic electronics, *Anal. Bioanal. Chem.* **406**, 2231 (2014).
- [27] H. Yoshida, Principle and application of low energy inverse photoemission spectroscopy: A new method for measuring unoccupied states of organic semiconductors, *J. Electron Spectrosc. Relat. Phenom.* **204**, 116 (2015).
- [28] L. Hedin, New method for calculating the one-particle Green's function with application to the electron-gas problem, *Phys. Rev.* **139**, A796 (1965).
- [29] M. M. Rieger, L. Steinbeck, I. D. White, H. N. Rojas, and R. W. Godby, The GW space-time method for the self-energy of large systems, *Comput. Phys. Commun.* **117**, 211 (1999).
- [30] L. Steinbeck, A. Rubio, L. Reining, M. Torrent, I. D. White, and R. W. Godby, Enhancements to the GW space-time method, *Comput. Phys. Commun.* **125**, 105 (2000).
- [31] C. Freysoldt, P. Eggert, P. Rinke, A. Schindlmayr, R. W. Godby, and M. Scheffler, Dielectric anisotropy in the GW space-time method, *Comput. Phys. Commun.* **176**, 1 (2007).
- [32] T. Wang, T. R. Kafle, B. Kattel, Q. Liu, J. Wu, and W.-L. Chan, Growing ultra-flat organic films on graphene with a face-on stacking via moderate molecule-substrate interaction, *Sci. Rep.* **6**, 28895 (2016).
- [33] H. Yoshida, Note: Low energy inverse photoemission spectroscopy apparatus, *Rev. Sci. Instrum.* **85**, 016101 (2014).
- [34] W. H. Lee, J. Park, S. H. Sim, S. Lim, K. S. Kim, B. H. Hong, and K. Cho, Surface-directed molecular assembly of pentacene on monolayer graphene for high-performance organic transistors, *J. Am. Chem. Soc.* **133**, 4447 (2011).
- [35] See Supplemental Material at <http://link.aps.org/supplemental/10.1103/PhysRevB.102.125302> for the XPS results [44,45], GIXD results [46], background subtraction from the spectra, details of the first-principle calculation methods [47–58], the calculated electrostatic energies, and the results of the mixed monolayer of CuPc and F₁₆CuPc [59,60].
- [36] H. Jiang, P. Hu, J. Ye, R. Ganguly, Y. Li, Y. Long, D. Fichou, W. Hu, and C. Kloc, Hole mobility modulation in single-crystal metal phthalocyanines by changing the metal- $\pi/\pi-\pi$ interactions, *Angew. Chem. Int. Ed.* **57**, 10112 (2018).
- [37] H. Jiang, J. Ye, P. Hu, F. Wei, K. Du, N. Wang, T. Ba, S. Feng, and C. Kloc, Fluorination of metal phthalocyanines: Single-crystal growth, efficient *n*-channel organic field-effect transistors, and structure-property relationships, *Sci. Rep.* **4**, 7573 (2014).
- [38] D. Schlettwein, K. Hesse, N. E. Gruhn, P. A. Lee, K. W. Nebesny, and N. R. Armstrong, Electronic energy levels in individual molecules, thin films, and organic heterojunctions of substituted phthalocyanines, *J. Phys. Chem. B* **105**, 4791 (2001).
- [39] H. Yamane and N. Kosugi, Substituent-Induced Intermolecular Interaction in Organic Crystals Revealed by Precise Band-Dispersion Measurements, *Phys. Rev. Lett.* **111**, 086602 (2013).
- [40] M. J. Frisch, G. W. Trucks, H. B. Schlegel, G. E. Scuseria, M. A. Robb, J. R. Cheeseman, G. Scalmani, V. Barone, G. A. Petersson, H. Nakatsuji, X. Li, M. Caricato, A. V. Marenich, J. Bloino, B. G. Janesko, R. Gomperts, B. Mennucci, H. P. Hratchian, J. V. Ortiz, A. F. Izmaylov *et al.*, GAUSSIAN 16, REV. B.01.
- [41] A. A. Goodwin, J. R. Atkinson, J. N. Hay, and F. W. Mercer, Dielectric relaxation behaviour of fluorinated aromatic poly(ether)s and poly(ether ketone)s, *Polymer* **40**, 1515 (1999).
- [42] F. Aryasetiawan and O. Gunnarsson, The GW method, *Rep. Prog. Phys.* **61**, 237 (1998).
- [43] D. Golze, M. Dvorak, and P. Rinke, The GW compendium: A practical guide to theoretical photoemission spectroscopy, *Front. Chem.* **7**, 377 (2019).
- [44] M. P. Seah and W. A. Dench, Quantitative electron spectroscopy of surfaces: A standard data base for electron inelastic mean free paths in solids, *Surf. Interface Anal.* **1**, 2 (1979).
- [45] C. D. Wagner, W. M. Riggs, L. E. Davis, and J. F. Moulder, *Handbook of X-Ray Photoelectron Spectroscopy* (PerkinElmer, Eden Prairie, Minnesota, 1979).

- [46] A. Opitz, B. Ecker, J. Wagner, A. Hinderhofer, F. Schreiber, J. Manara, J. Pflaum, and W. Brütting, Mixed crystalline films of co-evaporated hydrogen- and fluorine-terminated phthalocyanines and their application in photovoltaic devices, *Org. Electron.* **10**, 1259 (2009).
- [47] Y. Morikawa, H. Ishii, and K. Seki, Theoretical study of *n*-alkane adsorption on metal surfaces, *Phys. Rev. B* **69**, 041403 (2004).
- [48] M. Otani and O. Sugino, First-principles calculations of charged surfaces and interfaces: A plane-wave nonrepeated slab approach, *Phys. Rev. B* **73**, 115407 (2006).
- [49] I. Hamada, M. Otani, O. Sugino, and Y. Morikawa, Green's function method for elimination of the spurious multipole interaction in the surface/interface slab model, *Phys. Rev. B* **80**, 165411 (2009).
- [50] D. Vanderbilt, Soft self-consistent pseudopotentials in a generalized eigenvalue formalism, *Phys. Rev. B* **41**, 7892 (1990).
- [51] N. Troullier and J. L. Martins, Efficient pseudopotentials for plane-wave calculations, *Phys. Rev. B* **43**, 1993 (1991).
- [52] S. Grimme, Semiempirical GGA-type density functional constructed with a long-range dispersion correction, *J. Comput. Chem.* **27**, 1787 (2006).
- [53] A. Schindlmayr, Analytic evaluation of the electronic self-energy in the GW approximation for two electrons on a sphere, *Phys. Rev. B* **87**, 075104 (2013).
- [54] A. V. Krukau, O. A. Vydrov, A. F. Izmaylov, and G. E. Scuseria, Influence of the exchange screening parameter on the performance of screened hybrid functionals, *J. Chem. Phys.* **125**, 224106 (2006).
- [55] J. Heyd, G. E. Scuseria, and M. Ernzerhof, Hybrid functionals based on a screened Coulomb potential, *J. Chem. Phys.* **118**, 8207 (2003).
- [56] J. Heyd, G. E. Scuseria, and M. Ernzerhof, Erratum: Hybrid functionals based on a screened Coulomb potential [*J. Chem. Phys.* **118**, 8207 (2003)], *J. Chem. Phys.* **124**, 219906 (2006).
- [57] S. Sharifzadeh, A. Biller, L. Kronik, and J. B. Neaton, Quasi-particle and optical spectroscopy of the organic semiconductors pentacene and PTCDA from first principles, *Phys. Rev. B* **85**, 125307 (2012).
- [58] S. Refaely-Abramson, S. Sharifzadeh, M. Jain, R. Baer, J. B. Neaton, and L. Kronik, Gap renormalization of molecular crystals from density-functional theory, *Phys. Rev. B* **88**, 081204(R) (2013).
- [59] M. J. Frisch, G. W. Trucks, H. B. Schlegel, G. E. Scuseria, M. A. Robb, J. R. Cheeseman, G. Scalmani, V. Barone, G. A. Petersson, H. Nakatsuji, X. Li, M. Caricato, A. Marenich, J. Bloino, B. G. Janesko, R. Gomperts, B. Mennucci, H. P. Hratchian, J. V. Ortiz, A. F. Izmaylov *et al.*, GAUSSIAN 09, REV. A.02.
- [60] S. A. Abd-Rahman, T. Yamaguchi, S. Kera, and H. Yoshida (unpublished).